Influence of X-Ray Irradiation During Photoemission Studies on Halide Perovskite-Based Devices

Maryline Ralaiarisoa, Johannes Frisch, Mathieu Frégnaux, Stefania Cacovich, Armelle Yaïche, Jean Rousset, Mihaela Gorgoi, Davide R. Ceratti, Tim Kodalle, Fabrice Roncoroni, et al.

DOI: 10.1002/ ((please add manuscript number))

Article type: Full Paper

Influence of X-ray irradiation during photoemission studies on halide perovskite-based devices

*Maryline Ralaiarisoa, Johannes Frisch, Mathieu Frégnaux, Stefania Cacovich, Armelle Yaïche, Jean Rousset, Mihaela Gorgoi, Davide R. Ceratti, Tim Kodalle, Fabrice Roncoroni, Jean-François Guillemoles, Arnaud Etcheberry, Muriel Bouttemy, Regan G. Wilks, Marcus Bär, Philip Schulz**

M. Ralaiarisoa, S. Cacovich, D. R. Ceratti, J.-F. Guillemoles, P. Schulz

Centre National de la Recherche Scientifique, Institut Photovoltaïque d'Île-de-France

18 Boulevard Thomas Gobert, 91120 Palaiseau

E-mails: marylineralaiarisoa@yahoo.com, philip.schulz@cnrs.fr

J. Frisch, R. G. Wilks, M. Bär

Department of Interface Design, Helmholtz-Zentrum Berlin für Materialien und Energie GmbH, Albert-Einstein-Str. 15, 12489 Berlin, Germany

R. G. Wilks, M. Gorgoi, M. Bär

Energy Materials In-situ Laboratory Berlin (EMIL), Helmholtz-Zentrum Berlin für Materialien und Energie GmbH, Albert-Einstein-Str. 15, 12489 Berlin, Germany

M. Bär

Helmholtz Institute Erlangen-Nürnberg for Renewable Energy (HIERN), Albert-Einstein-Str. 15, 12489 Berlin, Germany

M. Bär

Department of Chemistry and Pharmacy, Friedrich-Alexander-Universität Erlangen-Nürnberg (FAU), Egerlandstr. 3, 91058 Erlangen, Germany

M. Frégnaux, A. Etcheberry, M. Bouttemy

Institut Lavoisier de Versailles, Université de Versailles Saint-Quentin-en-Yvelines

45 Avenue des États Unis, 78000 Versailles, France

A. Yaïche, J. Rousset

Électricité de France, Institut Photovoltaïque d'Île-de-France

18 Boulevard Thomas Gobert, 91120 Palaiseau, France

D. R. Ceratti

Sorbonne Université, CNRS, Collège de France, UMR 7574, Chimie de la Matière Condensée de Paris, 75005 Paris, France

T. Kodalle, F. Roncoroni

Molecular Foundry, Lawrence Berkeley National Laboratory,

1 Cyclotron Road, Berkeley, CA-94720, USA

Keywords: perovskite, photoelectron spectroscopy, X-ray, devices, beam, damage, flux

Abstract

Metal halide perovskites (MHPs) are semiconductors with promising application in optoelectronic devices, particularly, in solar cell technologies. The chemical and electronic properties of MHPs at the surface and interfaces with adjacent layers dictate charge transfer within stacked devices and ultimately the efficiency of the latter. X-ray photoelectron spectroscopy (XPS) is a powerful tool to characterize these material properties. However, the X-ray radiation itself can potentially affect the MHP and therefore jeopardize the reliability of the obtained information. In this work, we assess the effect of X-ray irradiation on $Cs_{0.05}MA_{0.15}FA_{0.8}Pb(I_{0.85}Br_{0.15})_3$ (MA for CH_3NH_3, and FA for $CH_2(NH_2)_2$) MHP thin-film samples in a half-cell device. We compared measurements acquired with synchrotron radiation,

and a conventional laboratory source for different times. Changes in composition and core levels binding energies are observed in both cases, indicating a modification of the chemical and electronic properties. Our results indicate that changes observed over minutes with highly brilliant synchrotron radiation are likely occurring over hours when working with a lab-based source providing a lower photon flux. We discuss the possible degradation pathways, supported by steady-state photoluminescence analysis. The work stresses the importance of beam effect assessment at the beginning of XPS experiments of MHP samples.

1. Introduction

The application of metal halide perovskite (MHP) semiconductors in solar cells have led to power conversion efficiency well beyond 25 %,[1] and over 32 % in tandem configuration.[2] MHPs are a class of materials crystallizing in the ABX_3 structure, where A is a monovalent organic, or a combination of organic and inorganic cation, B is a divalent metal cation, and X is a halide or multiple halide anions. These materials feature an exceptional combination of properties, i.e., dynamic disorder,[3] low exciton binding energy for spontaneous free charge carrier generation,[4,5] tunable optoelectronic properties,[6–8] and defect tolerance or self-healing capabilities.[9,10] The long-term application and viability of these materials as an active layer in solar cells require clear understanding of their optoelectronic properties, particularly at the interface to other functional layers in the solar cell. Specifically, the electronic properties of the MHPs and the energetics at the interfaces govern charge transfer at the interfaces and throughout the different layers of the device. It is therefore essential to assess the surface electronic properties of MHPs and their interfaces with adjacent functional layers. Substantial effort has been done in the past to determine the energy level alignment between the MHP and standard or potential charge transport as well as buffer layers by means of photoelectron spectroscopy (PES).[11–13] Unfortunately, the approach comes with pitfalls such as ambiguity in band onset determination,[14] substrate effects,[15,16] surface defects,[17] or surface contamination.[18]

A particularly crucial aspect during a PES study is the effect of illumination and X-ray irradiation on material properties.[19,20] Indeed, beam damage and irradiation-induced degradation can be significant,[9,21] and can be the source for inconclusive or misleading results. Complications range from surface photovoltage formation during the measurement[22] to structural dissociation of the perovskite structure via ion migration, decomposition, and/or effusion. The latter complication is particularly challenging for MHPs consisting of several

compounds like the multi-cation mixed halide perovskites. The impact can be even higher for synchrotron-based studies, where the photon flux can be several orders of magnitude higher than for standard laboratory-based X-ray sources. However, careful monitoring of the transient changes in the XPS data during acquisition yield deeper insights into fundamental materials properties and aid in the understanding of degradation behavior, as in photochemical and thermal degradation,[23] or even uncover self-healing properties.[24]

Here, we present a dedicated investigation of beam damage effects on MHP by carrying out PES studies employing synchrotron and laboratory light sources. Our study yields guidelines for precautions necessary to assess more reliably energy level positions and chemical composition of MHP surfaces and interfaces by PES. Furthermore, our results suggest degradation pathways for multi-cation mixed halide perovskites when exposed to an X-ray photon flux. Notably, monitoring these X-ray induced degradation processes further elucidates the cause of inherent instability of MHPs and thus set guidelines for effective damage mitigation and stabilization measures; either through adaptation of the complex MHP composition or by tailoring the interfaces to adjacent buffer and transport layers.

2. Results and Discussion

In the scope of this work, we primarily investigate the effect of X-ray exposure during photoemission experiments under synchrotron and laboratory-based irradiation on MHPs. For this purpose, triple cation mixed halide perovskite thin films with the nominal composition $Cs_{0.05}MA_{0.15}FA_{0.8}Pb(I_{0.85}Br_{0.15})_3$ (MA for methylammonium CH_3NH_3, and FA for formamidinium $CH_2(NH_2)_2$) were prepared as in an n-i-p perovskite solar cell but limited to a half-cell layer stack of glass/FTO/TiO_2/perovskite. Further details of the sample preparation can be found in the experimental section and SI. In the case of the synchrotron experiment, a comb-like gold electrode with fingers crossing the sample was deposited on top, as pictured in **Figure 1a**, for additional grounding and binding energy calibration. However, the XPS scans were taken on the exposed, bare perovskite surface, as for instance indicated by the white rectangular mark for the beam spot (Figure 1a) in the first synchrotron-based experiment.

First, we tested the long-term stability of the perovskite sample under synchrotron radiation in the soft X-ray regime (1000 eV photon energy), thus evaluating transient shifts of core level binding energies and changes to chemical composition. Second, we conducted laboratory-based XPS measurements (1487 eV photon energy) on similar perovskite samples to compare the previous findings to potential X-ray irradiation-induced degradation of the MHP films at lower X-ray photon flux conditions, thus capturing the initial stages of decomposition. We

complement this evaluation by correlating changes in composition due to beam damage with the optoelectronic properties of the beam-exposed area via microscopic photoluminescence (PL) measurements in the X-ray beam-exposed spot in a hyperspectral imaging (HSI) setup.[25]

2.1. Synchrotron-based XPS on triple-cation mixed halide perovskite devices

We begin by closely inspecting data that had been continuously taken in one beam spot for a I 3d-Pb 4f cycle, where one cycle consists of consecutively acquiring one scan (i.e., spectrum) of I 3d and Pb 4f core levels over the course of about 13 min (duration of I 3d-Pb 4f cycle times number of cycles). Selected spectra acquired throughout the XPS measurements at 0 min (1^{st} scan), approximately 4 min (4^{th} scan), and approximately 13 min (last, i.e., 12^{th} scan), for I $3d_{5/2}$, and Pb 4f are shown in **Figure 1b** and **Figure 1c**, respectively. Although the whole I 3d binding energy (BE) range has been acquired, only the I $3d_{5/2}$ BE region is shown in the figure for a clearer view. Most prominently, transient changes in the binding energy peak positions occur within minutes of beam exposure. Additionally, the intensities, (integrated area underneath photopeak), change over time with an evolution in the I/Pb peak intensity ratio, indicating transient changes to the relative concentration of iodine and lead in the probed sample volume (**Figure 1d)**.

These initial observations are further corroborated by a detailed analysis of the evolution over time of the BE positions and the shapes of the I $3d_{5/2}$ and Pb $4f_{7/2}$ core levels, summarized in **Figure 1e** and **Figure 1f**, respectively. The first cycle of measurement yields BE position at 619.8 eV, and 138.6 eV for I $3d_{5/2}$, and Pb $4f_{7/2}$, respectively. Within about 13 min, the core levels are shifted by up to 0.4 eV towards lower BE. This is in contrast to results of X-ray irradiation on methylammonium lead iodide $MAPbI_3$, where it was presumed that the generation of Pb donor states, i.e. undercoordinated and elemental lead, at the surface leads to Fermi level pinning close to the conduction band, presumably resulting in a shift of the core levels to higher binding energies.[20,26] Indeed, the Pb $4f_{7/2}$ spectra in our case does not exhibit any low BE contribution at ca. 137 eV attributable to elemental Pb. The described core level shift occurs continuously over time without significant change in full width at half maximum (FWHM), indicating a rigid shift. The core level position appears to converge to a stable value over time.

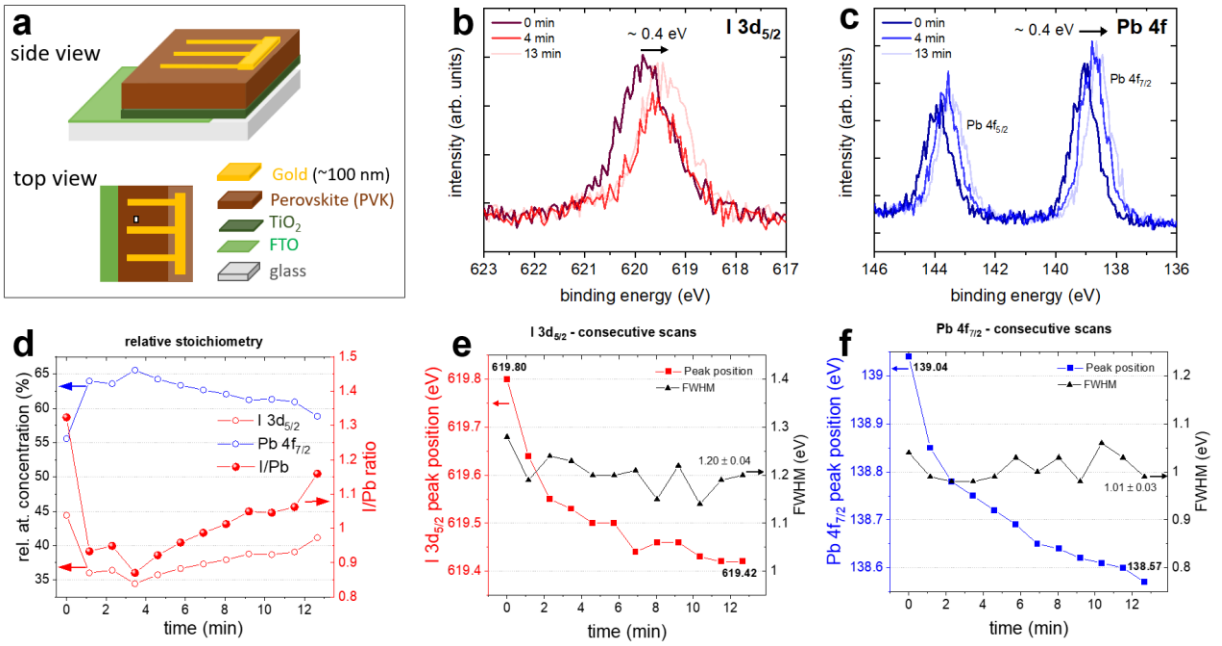

Figure 1. Synchrotron-based XPS of I 3d and Pb 4f core levels of sample 1 acquired over time. **a)** Schematics representing the half-cell sample design from a side and top view, the white square on the top view approximates the measurement spot (not to scale). Selected **b)** I $3d_{5/2}$ and **c)** Pb $4f_{7/2}$ XPS core level spectra after different irradiation times. **d)** Evolution of the relative concentration of iodine and lead and derived I/Pb ratio. The FWHM and binding energy (BE) peak position extracted from the fits applied to the spectra are shown for **e)** I $3d_{5/2}$ and **f)** Pb $4f_{7/2}$ over the course of data collection.

The changes in composition illustrated in **Figure 1d** highlight a significant drop in I/Pb ratio from 1.3 to 0.9 already after the first I 3d-Pb 4f cycle, i.e., within 2 minutes. The displayed values are to be interpreted as relative ratios, obtained by taking into consideration the linearly interpolated photoionization cross section of the photoelectrons from the respective core level and their estimated inelastic mean free path (IMFP) for our measurement, based on [27–29]. We note that the values of the I/Pb ratio exhibit a significant deviation from the expected value 2.55 (2.5 if considering the 10% excess of PbI_2 in the preparation). This abrupt decrease of the I/Pb ratio after the first measurement cycle points toward a rapid drop in the iodine content, e.g. via effusion of I or halide segregation, occurring as soon as the sample is exposed to X-rays, i.e., as the first spectra were acquired, such that the changes would not be detected on the time scale of the measurement. Importantly, after about 5 min, the I/Pb ratio increases again over time towards the initial value, suggesting a rearrangement of the surface composition.

2.1.2. Influence of synchrotron X-ray relative intensity

To better capture the initial stages of these X-ray induced degradation mechanisms, we have repeated measurements with systematically reduced beam intensity. For a more concise understanding of potential halide segregation processes, we conducted these adjusted XPS measurements on another $Cs_{0.05}MA_{0.15}FA_{0.8}Pb(I_{0.85}Br_{0.15})_3$ MHP, labelled sample 2, in a Pb 4f-I 3d-Br 3d cycle over time. For each selected beam intensity, the scans of Pb 4f, I $3d_{5/2}$, and Br 3d are acquired in a new beam spot which was not previously exposed to radiation. The most significant markers for changes to the MHP film are the core level peak positions. The corresponding BE shifts relative to the first sweep over time is depicted in **Figure 2**. The representation of the same data as absolute BE shift can be found in Figure S2a. We observed a general trend where the core levels shift to lower BE value for all beam intensities until a definite binding energy position is reached, as also observed for sample 1 (see Figure 1).

Additionally, the longer exposure times used in this measurement series reveal that, after reaching this maximum shift, the core level shifts back to higher binding energy values. For lower beam intensity the initial shift for each respective core level occurs more gradually and the shift back toward higher BE sets in at a later stage, as best seen for the I $3d_{5/2}$ and Pb $4f_{7/2}$ core levels. Notably, the data for the Br $3d_{5/2}$ core level exhibits a lower signal-to-noise ratio due to the smaller photoionization cross-section, but the changes track the one observed in the iodine core levels within the margin of error in this measurement. Small changes in this behavior are observed for lower beam intensities, for which the shifts in the bromine core levels are slightly more pronounced. This could be related to different kinetics of the different degradation processes such as for instance thermal degradation and photochemically induced halide segregation, the latter being particularly relevant for changes in the halide core level shifts.[23,30,31] For easier visualization, we mark the turning point, i.e., the time when the transient shift to lower binding energies converts back to a shift to higher binding energies, as a dashed line in Figure 2 (see also Figure S2a). We evaluated the respective turning point by determining the local minimum from polynomial fits of the data around the turning point. The time shift between the turning points at different beam intensities illustrates the dependence of the BE shift on the X-ray fluence, as also evidenced with the representation of the BE position as a function of the fluence shown in Figure S2b. Indeed, Figure S2 highlights how the turning point overlaps for all fluences. Whereas all core levels follow a similar trend in terms of binding energy shift, the magnitude of the shift between different core levels in the same measurement

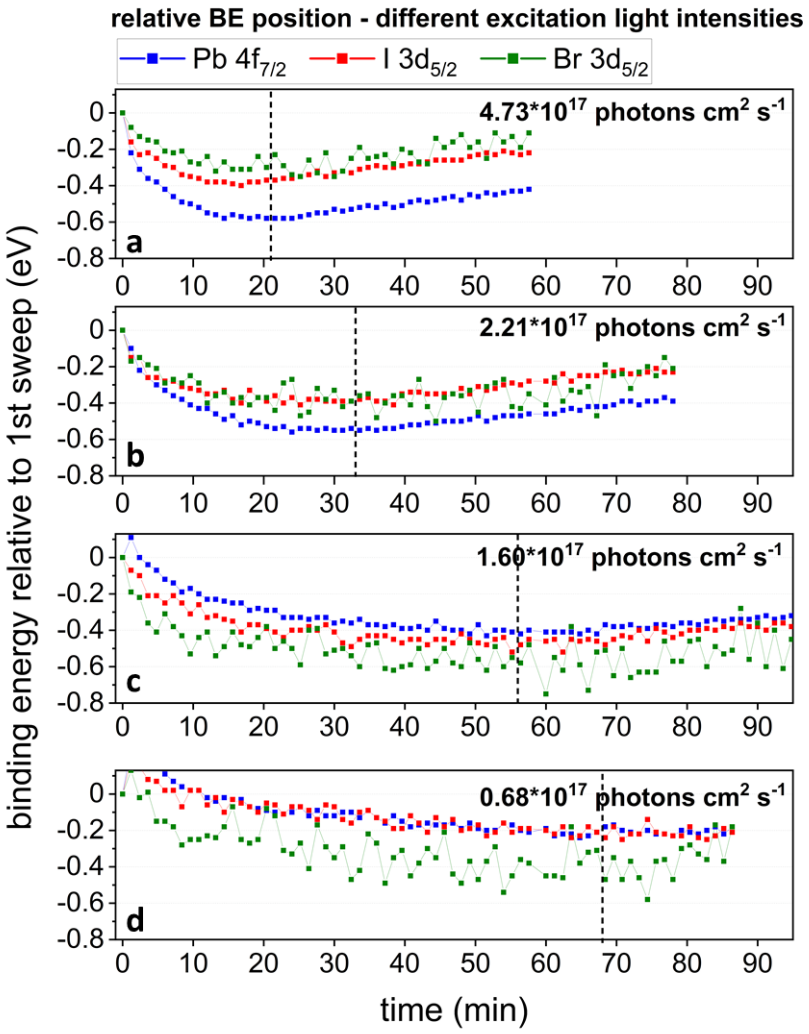

Figure 2. Synchrotron-based XPS data of sample 2 acquired over time in a Pb 4f-I 3d-Br3d cycle and for different excitation light intensities. X-ray induced BE shift relative to the first sweep (time=0 min) are shown after being calculated based on the fits applied to the Pb $4f_{7/2}$ (blue), I $3d_{5/2}$ (red), and Br $3d_{5/2}$ (green) core level spectra. The X-ray intensities are expressed in terms of approximate photon flux in photons·cm^2·s^{-1}; (a) the highest intensity, (b) 1/2, (c) 1/3, and (d) 1/7 of the highest intensity. The vertical, dashed lines indicate the average turning point when the peak position shifts back to higher BE values for the respective relative intensities. Alternative representations of the same data for each core level with the absolute binding energy values can be found in Figure S2.

cycle differs between lead and the halides (I and Br), particularly in the case of the highest beam intensities (Figure 2a). Indeed, by using a beam with an approximate beam flux of 4.73 x 10^{17} photon cm^{-2} s^{-1} the maximum shift amounts to about 0.6 eV for Pb 4f and up to 0.4 eV for I 3d and Br 3d around the turning point. This BE offset is occurring from the start and is decreasing

in magnitude with decreasing beam flux to ~2.21, to 1.6, to 0.68 x 10^{17} photon cm^{-2} s^{-1} (Figure 2b-2d), and is negligible for the two lowest beam intensities, especially for Pb 4f and I 3d.

The degradation processes become clearer when tracking changes in composition on the MHP sample 2 surface (see **Figure 3**). In addition to the significant changes in the iodine to lead ratio we also look at the halide mixing ratio in the sampled area. The higher the beam intensity, the more pronounced are the changes. After an initial drop in I/Pb and I/Br ratios, we observe a slight but steady increase for both ratios over time indicating an enrichment of the surface in iodine. This is unexpected at first as in the past, effusion of the more volatile organic species on the perovskite A-site and iodine resulted in the conversion of perovskites into the corresponding lead-dihalides, i.e., PbI_2 or $PbBr_2$.[9] However, a direct comparison of the total halide to lead ratios, i.e., (I+Br)/Pb, in Figure 3b shows much less pronounced changes with exposure time, which indicates that the initial drop in the iodine content is related to halide segregation akin to halide segregation observed under light exposure.[32,33]

Importantly, the initial I/Br ratio is overall below 2, much lower than the expected 5.7, which further corroborates the rapid loss of iodine at the beginning of the XPS measurement/exposure as discussed in 2.1.1. The increase of the I/Br ratio with longer exposure time then indicates a (partial) reversal of this effect. This is in line with previous reports that found experimental evidence for the segregation of I and Br in $MAPbI_{3-x}Br_x$ upon illumination.[33] Interestingly, the various spots in our experiment exhibit different stoichiometries for the initial measurement and hence starting conditions for each series of scans. We highlight that the time when the concomitant increase in I/Pb and I/Br ratio reaches a saturation corresponds to the turning point when the core levels shift back to higher binding energies (see Figure 2). This implies a correlation between the chemical composition and the electronic properties at the surface of the sample, even though the observed trend remains universally true for various initial (I+Br)/Pb ratios. This is similar to earlier observations of substrate-dependent core level shifts of halide perovskites that showed the same order of magnitude, irrespective of their surface

composition.[29] Also the discrepancy between the Pb and halide core level shifts, observed in our experiments with performed at the higher beam flux, track with the changes in the I/Pb and I/Br ratio, which is consistent with a transient change of chemical coordination. Of note, the BE shift back to higher values after extended exposure could also in part be related to a charging effect, that is possibly linked to the material potentially becoming less conductive due to a phase change.

2.2. Laboratory-based XPS on triple-cation mixed halide perovskite devices

The results from the synchrotron-based XPS measurements suggest that further insight into the A-site cation and X-site anion distribution in the probed sample surface as a function of the radiation dose is required to fully attribute the transient chemical reaction and correlated optoelectronic changes. We thus expanded the characterization using further reduced beam

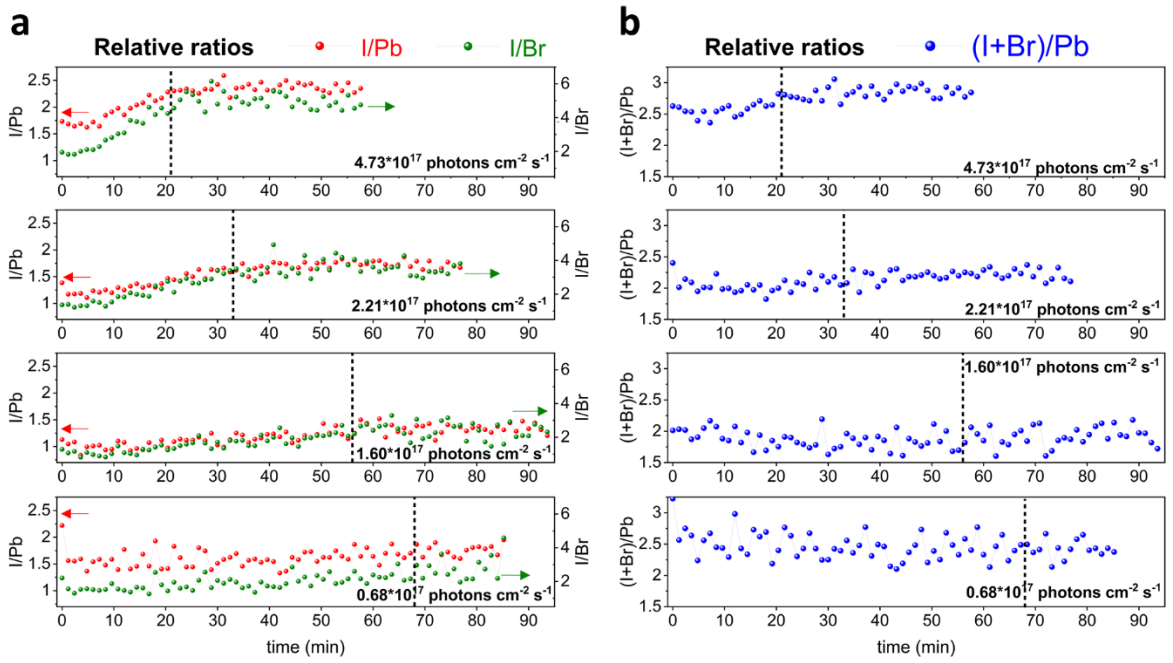

Figure 3. Synchrotron-based XPS on sample 2 during a series of consecutive scans acquired over time in a Pb 4f-I 3d-Br3d cycle and for different excitation light intensities. Evolution over time of (a) relative I/Pb (red) and I/Br (green) ratios and (b) of the halide relative content (I+Br)/Pb ratios (blue) extracted from the fits applied to Pb $4f_{7/2}$, I $3d_{5/2}$, and Br $3d_{5/2}$ core level spectra. The X-ray intensities from top to bottom panel are expressed in terms of photon flux in 10^{17} photons cm^{-2} s^{-1}, from the top to bottom panels: The highest intensity, 1/2, 1/3, and 1/7 of the highest intensity. The vertical, dashed lines indicate the time where the corresponding peak positions shift back to higher BE (see also Figure 2), and the time when I/Br ratio increasing trend ends.

intensity on the MHP by conducting XPS measurements with a laboratory-based X-ray source. We track the evolution of the core levels in a similar fashion as for the previous experiments at the synchrotron facility but with lower intensities; more precisely, the photon flux from the Al K_α source used is estimated as 5 x 10^{13} photon cm^{-2} s^{-1}. We expect more detailed information on the first stages of degradation via laboratory-based PES experiments, i.e., by mapping the onset of the degradation.

Representative spectra and their fits at selected time spans from the start to the end of the measurements after 520 min are shown in **Figure 4** for sample 3, having the same composition as the previous studied samples. Like samples 1 and 2, the selected core levels were acquired in a sequential manner in two measurement series: N 1s-I 3d-Pb 4f (**Figure 4a**) and Br 3d-I 3d-Cs 3d (**Figure 4b**), each series was acquired on a "fresh" spot, i.e. a location on the sample without former exposure to X-rays. Such acquisition sequence allows us to record transient changes for each core level peak with sufficient signal to noise ratio while keeping the time steps between two subsequent measurements of the same peak on the order of a few minutes. Summary of the fit results for the entire time series is shown in **Figure 5**; namely the BE position over time vs. the BE of the first spectrum (**Figure 5a-b**) and the relative atomic concentrations of the elements (**Figure 5c-d**). By selecting a comparable time frame for both cycles, we assume we can compare the behavior of all the selected core levels at a given time. It is important to stress, though, that whereas the changes in BE positions of core levels from different series can be related to each other, the evaluated concentrations are relative to those of the selected elements within the same series only.

N 1s in Figure 4a exhibits two peak contributions at 400.9 eV, and 402.7 eV, corresponding to nitrogen as in FA^+, and MA^+, respectively. We observe a lower intensity contribution from the MA^+, which results in a higher level of error in the determination of the related BE positions and spectral area (see Figure 5a, c). The same remark applies also for the modest contribution of undercoordinated Pb^{x+} ($x < 2$) situated at 137.7 eV (at t = 0), a lower binding energy (i.e., with lower oxidation state x) than Pb^{2+} from perovskite located at 138.8 eV (at t = 0). Pb^{x+} does not correspond to metallic lead,[34] which is expected at ~1 eV lower BE, and might rather be related to understoichiometric lead halide or lead oxide species.[35]

The I $3d_{5/2}$ core level is located at 619.6 eV in both series of measurements, confirming the reproducible measurements on two different analyzed areas of the sample. Figure 4b additionally shows the Br 3d spectra with the Br $3d_{5/2}$ peak position at 68.8 eV, and the Cs 3d spectra fitted over the Cs $3d_{5/2}$ BE range, centered at 725.3 eV at t = 0. The higher level of background noise of the Cs $3d_{5/2}$ spectra in Figure 4b results in larger variation within the fit parameters (see Figure 5d) and thus, allows mostly a qualitative evaluation of the data trend. *A priori*, all core levels exhibit an almost constant BE position up to 200 min, and then a pronounced BE shift to lower values between 200 min and 350 min. However, a closer look at the relative core level positions in Figure 5a-b evidences a minor but gradual shift (up to 0.1 eV) of all core levels towards lower binding energies within the first 70 min of X-ray exposure. From about 70 min to 200 min of X-ray exposure, the core levels reach a constant value and exhibit at most a few tens of meV shift, i.e., beyond the accuracy limit of the measurement. Finally, from t = 200 min on, we observed a continuous shift of all core levels towards lower

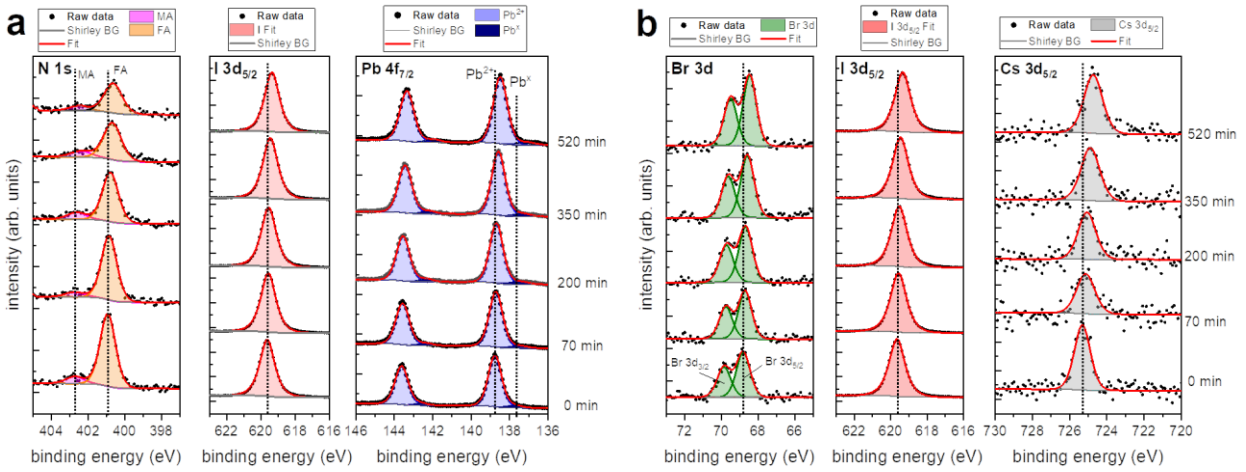

Figure 4. Laboratory-based XPS on sample 3 during series of 110 consecutive scans acquired over a total time of 520 min. Representative XPS spectra at selected times: 0 min (first scan), 70 min, 200 min, 350 min, and 520 min (last scan), and corresponding fits of core levels acquired in **a)** N 1s-I 3d-Pb 4f cycle (N-I-Pb series), and **b)** Br 3d-I 3d-Cs 3d cycle (Br-I-Cs series) are shown. The N-I-Pb series and the Br-I-Cs were carried out on two different spots of the sample. BG stands for background. Vertical dotted lines are drawn to locate the BE position of each core level from the first scan. Note: The signal over the whole I 3d BE range has been acquired, only I $3d_{5/2}$ is shown here for enhanced overview.

binding energies (see Figure 5a,b). The trend persisted throughout the experiment, and no maximum shift was reached by the end of the measurement.

Relative atomic concentrations in Figure 5c displays a gradual and concomitant increase of the I and Pb concentrations, and a gradual decrease of the relative FA content over the whole duration of the measurements and concomitant X-ray exposure. MA exhibits a low and stable relative concentration up to around t = 100 min, where its relative concentration increases and reaches a steady value at around the 190 min mark, just before t = 200 min. The trend in the relative content of Br, I, and Cs to each other in Figure 5d can be distinguished over three

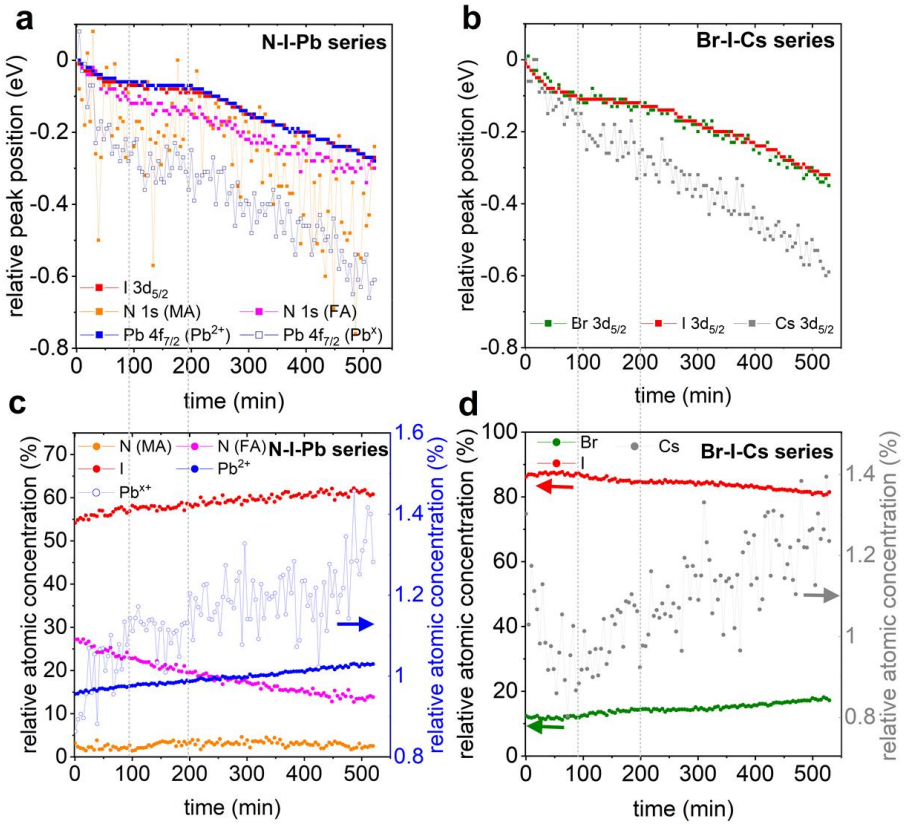

Figure 5. Laboratory-based XPS on sample 3 during series of 110 consecutive scans acquired over time. Evolution over time of BE position for spectra acquired consecutively for **a)** N 1s (MA) – orange, N 1s (FA) – magenta, Pb $4f_{7/2}$ for Pb^{2+} – blue full square, Pb $4f_{7/2}$ for Pb^{x} – dark blue open square, and I $3d_{5/2}$ – red, in a N 1s-I 3d-Pb 4f cycle (N-I-Pb series) and **b)** for Br $3d_{5/2}$ – green, I $3d_{5/2}$ – red, and Cs $3d_{5/2}$ – grey, in a Br 3d-I 3d-Cs 3d cycle (Br-I-Cs series). The dotted vertical lines indicate the time corresponding to the selected spectra in Figure 4. Correspondingly, relative atomic concentration of **c)** of I – red), N (MA) – orange, N (FA) – magenta, I – red, Pb^{2+} – blue full circle, Pb^{x+} – blue open circle, for the N-I-Pb series and **d)** of Br – green), I – red, and Cs (grey) for the Br-I-Cs series. The vertical dashed lines indicate the three regimes for $0 < t_1 < 100$ min, 100 min $< t_2 <$ 200 min, and 200 min $< t_3$.

regimes (visually separated by vertical gray lines) for the timespans: t < 100 min (Regime I), 100 min < t < 200 min (Regime II), and after 200 min (Regime III). In regime I, Br and I exhibit stable relative concentrations, whereas the scattered Cs concentration points to a decrease. From ca. t=100 min on, the latter features a continuous increase, while Br and I rather exhibit a mirrored trend with a relative increase and decrease, respectively. The Br and I trends display different slopes before and after t=200 min, which coincides with the time when the core levels start to further shift to lower BE (Figure 5a-b). Additional structural data can be insightful to further interpret the degradation behavior of the perovskite and reveal the appearance of new crystallographic phases and degradation products. In particular, degradation behavior of halide perovskites has been observed under typical measurement conditions in X-ray diffraction (XRD) measurements.[26,36] Here, we employed microdiffraction XRD experiments on the triple halide perovskite thin-films to test for significant structural changes. Note that the X-ray irradiation conditions are different from the ones in the XPS experiments as the photon energy was 10 keV for the microdiffraction experiment and data acquired in grazing-incidence wide angle X-ray scattering (GIWAXS) geometry under an incident angle of 0.5° in inert gas atmosphere. Even though the X-ray absorption profile in the perovskite film is thus different from the one in the XPS measurements, the experiment would still elucidate structural changes. The diffraction pattern at the beginning and at the end of the 3 h measurement, which corresponds to the order of magnitude of radiation dose in the lab-based XPS measurement, do not indicate any major change in the crystal structure or texture of the bulk perovskite material (see supplementary information, figure S4a,b). The extracted, quantitative data suggest a minor shift of the (100)-perovskite peak towards higher q values, indicating a slight contraction of the lattice spacing). The area under the curve of the (100)-perovskite peak, however, decreases by around 10% during the first hour of the experiment indicating a slight degradation of the thin film.

2.3. Discussion

2.3.1. Interpreting the effects of synchrotron vs. laboratory light source from XPS data

Our results evidence enhanced material degradation with the four orders of magnitude higher photon fluxes used during synchrotron experiments, compared to lab-based experiments. Although we observe gradual shifts of the core levels to lower BE in both cases, the time scale on which the shifts occur depends on the photon intensity. With synchrotron radiation, we observe a BE shift which saturates at values of up to -0.6 eV within 10-20 min and reverses direction thereafter, whereas the exposure to lab-based source leads to only a few tens of meV

shift on the same time scale, and most of the core levels exhibit only a shift of -0.4 eV after more than 8 hours. Obviously, the rate of BE shift is directly linked to the extent of exposure over time, i.e., to the x-ray fluence (Figure S2), however in the current experiment it cannot be determined whether the lab-based measurements would eventually have exhibited the same saturation and reversal as observed in the synchrotron-based measurements.

Therefore, we propose that the degradation observed during synchrotron experiments represents a "time-lapse" of the degradation induced by lab-based sources during photoemission experiments. We observe a rapid drop of the relative iodine content within a few minutes upon synchrotron irradiation, while such a drop starts to set in only after >100 min under X-ray exposure with a lab source. Decreasing the beam intensity weakens the effects but does not prevent the degradation in the long-term. The instant emission, and simultaneously observed transparent area from the X-ray spot during synchrotron measurements indicates that the degradation consists in a phase segregation into larger band-gap materials. This stresses the importance of visually or optically checking MHP samples for potential degradation already in the first seconds of measurements during synchrotron experiments. We postulate that the interpretation of the lab-based results can provide indications of the different steps of the initial X-ray induced degradation of the mixed perovskite film that would be unattainable from the synchrotron experiments.

The different trends of BE shift and relative atomic concentrations from the lab-based XPS measurements can be narrowed down and correlated following three timespans. First, at the earlier stage of exposure up to t = 100 min (Regime I), the most pronounced loss of FA and Cs coincides with only a minor BE shift. Since the relative MA content remains stable, and a similar trend in relative Pb, I, and Br content is observed, we can suppose that the pristine perovskite structure is still preserved, and the FA and Cs loss translate only into defect states that seem to not affect the electronic properties in a significant manner yet. This reminds of the preserved electronic properties of $MAPbI_3$ despite the defects generation in the form of iodine and MA vacancies upon X-ray exposure.[9] Second, for 100 min < t < 200 min (Regime II), the lack of BE shift is accompanied by the onset of contrasting trends between I and Br, and a relative MA increase. We interpret this second timespan as a transition period when an increasingly significant change in the relative stoichiometry of the sample occurs and rearrangements of bonds for new phases formation likely start to set in. Third, from t=200 min on (Regime III), we indeed observe the same trend of the relative atomic concentrations as during the transition period, correlated with a continuous BE shift of all core levels. The change in relative stoichiometry likely corresponds to the gradual segregation of the pristine

$Cs_{0.05}MA_{0.15}FA_{0.8}Pb(I_{0.85}Br_{0.15})_3$ MHP film into different phases. This modification of the surface chemistry results in a more pronounced electronic property change – BE shift – due to the conversion of the initial mixed perovskite material into possibly larger band-gap materials. This explanation is supported by an onsetting trend in our PL data on a triple cation perovskite sample similarly exposed to X-ray in the next section 2.3.2.

It is noteworthy that over the course of the lab-source based experiments the low BE contribution Pb^{x+} tends to increase, whereas such contribution is not detected in the case of the synchrotron experiments. This indicates that the Pb^x formation is likely mediated by the gradual formation and conversion of the materials, processes which are accelerated or "overleapt" under synchrotron radiation. In the latter case, the overall core level shift to lower BE reaches a saturation after a few tens of minutes, which correlates with iodine content reaching a constant value relative to Br and Pb, likely indicating the advanced conversion of the exposed area into segregated phase(s). We tentatively link the subsequent BE shift back to a higher value to a potential charging of the degraded material at the exposed spot that likely has a lower conductivity than the pristine perovskite.

The changes in composition and BE shift are observed not only under synchrotron radiation but also under lab-source with lower intensity. Although radiation sources with tunable intensities can help attenuate the extent of the changes, changes can still be observed, which stress the importance of comparing the (first) sweeps of the different core levels at the beginning and during any XPS measurements on MHPs to assess any potential beam damage.

2.3.2. Photoluminescence imaging of X-ray exposed MHP device

To further assess the effect of laboratory-based X-ray irradiation on the optoelectronic properties of triple cation perovskite thin films we performed quantitative steady-state photoluminescence imaging analysis. **Figure 6a** shows the reconstructed PL signal of a series of images acquired at the gold/MHP boundary of sample 4 (of the same composition as the previous samples) including an area that had been exposed to lab-based X-ray radiation for 6 hours. The elliptical shape of the beam is clearly visible and highlighted by a dashed white line. The absolute PL signal, measured at approximately 1 sun equivalent illumination, gradually decreases from the edge towards the center of the ellipse, suggesting the presence of inhomogeneous beam-induced degradation phenomena within the XPS spot. In **Figure 6b** the average PL spectra of four regions ranging from the as-deposited perovskite thin film (zone 1) to the core of the spot (zone 4) are reported, showing a clear evolution in terms of both PL peak intensity and position.

The band gap is widening in the center of the XPS spot. Although the PL data predominantly provides information from the bulk, we would expect the modification induced by the X-ray observed here to also apply to the surface of the sample, which would, in that case, be in line with the previous consideration on the evolution of the I/Br ratio for lab-based XPS measurements showing a gradual loss of iodine over time, and hence the formation of a wide-gap Br-rich phase. The X-ray exposure has thus modified the optical behavior of the triple cation perovskite that however still maintains good emission properties. These PL results corroborate the phase segregation suggested by the XPS measurements. The distinct spatial differentiation of their optoelectronic properties is likely related to an intensity distribution of the beam, which is more intense at the center of the beam spot. This stresses the importance of the beam intensity on the extent of beam-induced phase segregation or degradation. Furthermore, an inhomogeneous beam intensity can gradually affect the exposed area and result

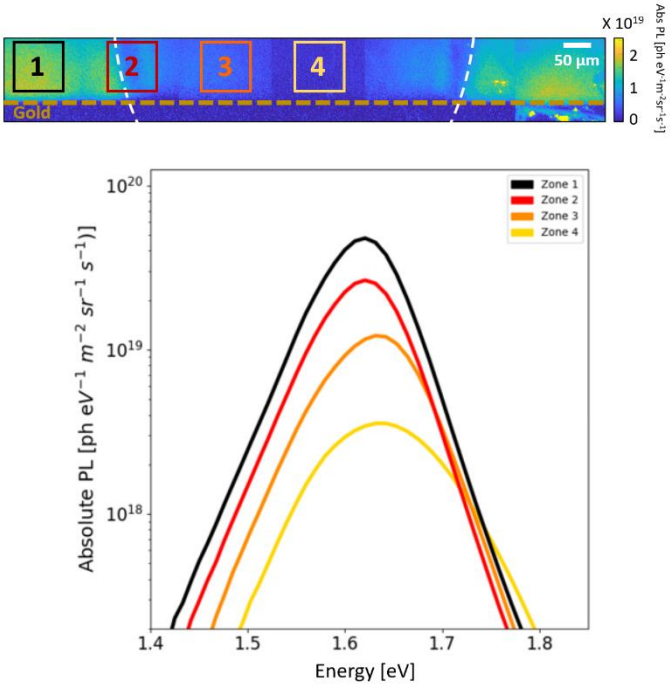

Figure 6. Top: reconstructed hyperspectral image from several square images of the investigated region across the X-ray exposed area of sample 4 (white dashed lines mimicking the shape of the X-ray spot). Bottom left: absolute PL spectra obtained from the integration of PL intensities over four different zones across the investigated X-ray exposed area, as shown by the squares in the top figure.

in spatially inhomogeneous material properties. This must particularly be kept in mind during XPS experiments since XPS spectra are usually built up from the average signal over an X-ray exposed area, and therefore the XPS data can erroneously lead to inaccurate interpretation. The inhomogeneity could for instance explain the transition period described in 2.3.1., when chemical modification (relative Br and MA increase) is observed – likely at the center of the beam spot –, whereas the electronic properties still appeared unaffected, likely due to the dominant still pristine perovskite around the center of the beam spot.

3. Conclusion

We investigated the influence of standard X-ray radiation used during XPS experiments, namely a standard Al K_α ($h\nu$ =1487 eV) laboratory-based source and ($h\nu$ = 1000 eV) synchrotron radiation, on the properties of a $Cs_{0.05}MA_{0.15}FA_{0.8}Pb(I_{0.85}Br_{0.15})_3$ MHP. The irradiation alters the electronic and chemical structure of these multi-cation MHPs and the extent of the alteration depends on the magnitude of the photon flux involved and the duration of the radiation exposure. The major alteration we observed is a gradual shift of the core levels towards lower binding energies, concomitant with a loss of iodine and organic compounds. From visual observation and supported by hyperspectral data, we interpret this alteration as a phase segregation. However, while a maximum BE shift of -0.6 eV is completed within less than 20 min with the different synchrotron photon fluxes used, the maximum BE shift is still not reached after more than 8 h of X-ray exposure with the standard laboratory source. Laboratory-based source attenuates the effects but does not prevent them. Within the first 70 min of laboratory-based measurement, a small but gradual BE shift up to 0.1 eV is already observed, accompanied by a loss of FA. Therefore, our findings also highlight minute shifts and chemical changes which can occur during XPS experiments, and which can be overseen while systematically acquiring several spectra for averaging, as is often the case during XPS experiments. Careful test measurements with individual scans and different X-ray photon fluxes should *a fortiori* be done to assess the beam-induced alterations of MHP during XPS.

4. Experimental Section

Sample Preparation: $Cs_{0.05}MA_{0.15}FA_{0.8}Pb(I_{0.85}Br_{0.15})_3$perovskite layers were synthetized following the same synthesis protocol as described and published in reference 30. Detailed configuration of the device and sample configuration can be found in SI (Figure S1).

After Au deposition by thermal evaporation as described in reference 30, sample 1 and sample 2 were briefly exposed to air before being stored in blind-flanged tubes in nitrogen atmosphere for transportation to the synchrotron or laboratory measurement sites.

Synchrotron-based XPS: Nitrogen-filled transport tubes were opened in a nitrogen-filled glove box at the synchrotron facility and stored there until the measurements. The MHP samples were transferred into the ultra-high vacuum (UHV, base pressure $<10^{-9}$ mbar) analysis chamber directly from the glove box without direct air exposure. The synchrotron measurements were carried out at the Energy Materials In-Situ Laboratory Berlin (EMIL) at BESSY II, HZB in Berlin, using the SISSY I end station at the soft X-ray beamline UE48 with linear horizontally polarized light. The XPS spectra were acquired with X-rays of 1000 eV photon energy, at the standard PGM (plane grating monochromator) c_{ff}-factor (exit and incident angles ratio) of 2.25 and using an exit slit of 30 µm. The photon focus size at SISSY I is 43 x 29 μm^2. The binding energy position of the spectra were calibrated by measuring the Au 4f core level spectra of a gold film on silicon sample and setting the Au $4f_{7/2}$ peak maximum to 84 eV (Figure S3, SI). The overall energy resolution is ca. 200 meV (FWHM). For the intensity-dependent experiment, the beam flux was decreased by changing the undulator gap size (i.e., detuning the energy of the undulator relative to that of the PGM) and monitoring the resulting photoelectron signal from an Au sample to determine the relative intensity (note that this procedure does not account for changes in the relative intensities of photons generated by other undulator harmonics that may reach the sample). The SISSY I endstation uses a ScientaOmicron EW4000 electron analyzer with an acceptance angle of ±25°, and the axis of the analyzer is ~50° from the incident beam direction (22.5° elevation, 45° rotation relative to the incoming beam). The angle of the sample normal relative to the incoming beam was approximately 45°, giving an emission angle relative to the central axis of the analyzer of 22.5°.

Laboratory-based XPS: Samples are briefly mounted at ambient air before being loaded into the laboratory-based XPS system. The XPS measurements were performed with the Nexsa XPS system of Thermo Fischer Scientific, using a monochromatic Al K_α source (1486.6 eV). The beam spot is an ellipse with a nominal minor axis of 400 µm. The source power selected for the measurement is 72 W.

X-ray Photoemission Spectroscopy (XPS) Analysis: The fitting of the XPS spectra was done using casaXPS. Quantitative analysis of the data acquired with the lab-source, the sensitivity factors specific to the system were used. For the quantitative analysis of the synchrotron data, the calculated areas were divided by the estimated IMFP,[29] and the photoionization cross-section σ of the respective core levels, which were linearly interpolated from the data in Trzhakovskaya et al..[27,28] One obtains a corrected value "area/(IMFP*σ)". The atomic concentration of an element x relative to the other considered elements is then obtained from: $at_x\% = (area_x/\sigma_x)/[\Sigma(area_i/\sigma_i)]$.

PL-HI:

The hyperspectral imaging (HI) system records a luminescence intensity signal along three dimensions {x,y,λ}. The set-up is composed by a home-built microscope with Thorlabs optomechanical elements, a 2D bandpass filtering system from company PhotonEtc with 2 nm resolution, and a 1Mpix silicon-based CCD camera PCO1300. The sample was illuminated (λ = 532 nm) through an infinity-corrected ×50 Nikon objective with numerical aperture of 0.85, and the luminescence is collected through the same objective. The excitation beam and luminescence signals are separated with appropriate dichroic beam splitter and filters. The 2D luminescence signal is corrected for each pixel of the sensor from the spectral transmissions along all the optical path, from the read noise and dark current noise of the camera. The acquisitions were performed in air atmosphere, at 40% RH and at temperature of 25°C.

.

XRD Microdiffraction: The GIWAXS data were collected at the 12.3.2 microdiffraction beamline of the Advanced Light Source (ALS) in a custom-made analytical chamber for a duration of 3 h. The incident angle of the incoming X-ray beam was set to 0.5° with a beam energy of 10 keV and a photon flux of about 10^9 photons/s and a beam footprint of about 5 microns by 110 microns. The GIWAXS data were recorded with an integration time of one second using a Pilatus 1 M 2D detector (Dectris Ltd.) and calibrated using an Al_2O_3 reference sample. Data evaluation and fitting was done using software written in house with GIWAXS-patterns being fitted using Gaussians profiles.

Supporting Information

Supporting Information is available from …

Acknowledgements

M. R. and P. S. thank the French Agence Nationale de la Recherche for funding under the contract number ANR-17-MPGA-0012. S.C. thanks funding from the European Union's Horizon 2020 research and innovation programme under the Marie Sk*łodowoska-Curie Grant Agreement N* 845612. We thank the Helmholtz-Zentrum Berlin für Materialien und Energie for the allocation of synchrotron radiation beamtime. This work was supported by User Projects at the Advanced Light Source (ALS, beamline 12.3.2) and at the Molecular Foundry, supported by the Office of Science and Office of Basic Energy Sciences of the US Department of Energy (contract DE-AC02-05CH11231). T. K. acknowledges funding via the U.S. Department of Energy, Office of Science, Office of Basic Energy Sciences, Materials Sciences and Engineering Division (D2S2 program KCD2S2). P. S., D. R. C. and T. K. thank the France-Berkeley Fund for funding support.

Received: ((will be filled in by the editorial staff))
Revised: ((will be filled in by the editorial staff))
Published online: ((will be filled in by the editorial staff))

[1] J. J. Yoo, G. Seo, M. R. Chua, T. G. Park, Y. Lu, F. Rotermund, Y.-K. Kim, C. S. Moon, N. J. Jeon, J.-P. Correa-Baena, V. Bulović, S. S. Shin, M. G. Bawendi, J. Seo, *Nature* **2021**, *590*, 587.
[2] A. Al-Ashouri, E. Köhnen, B. Li, A. Magomedov, H. Hempel, P. Caprioglio, J. A. Márquez, A. B. M. Vilches, E. Kasparavicius, J. A. Smith, N. Phung, D. Menzel, M. Grischek, L. Kegelmann, D. Skroblin, C. Gollwitzer, T. Malinauskas, M. Jošt, G. Matič, B. Rech, R. Schlatmann, M. Topič, L. Korte, A. Abate, B. Stannowski, D. Neher, M. Stolterfoht, T. Unold, V. Getautis, S. Albrecht, *Science* **2020**, *370*, 1300.
[3] K. T. Munson, E. R. Kennehan, G. S. Doucette, J. B. Asbury, *Chem* **2018**, *4*, 2826.
[4] A. Miyata, A. Mitioglu, P. Plochocka, O. Portugall, J. T.-W. Wang, S. D. Stranks, H. J. Snaith, R. J. Nicholas, *Nat. Phys.* **2015**, *11*, 582.
[5] V. D'Innocenzo, G. Grancini, M. J. P. Alcocer, A. R. S. Kandada, S. D. Stranks, M. M. Lee, G. Lanzani, H. J. Snaith, A. Petrozza, *Nat. Commun.* **2014**, *5*, 3586.
[6] J. H. Noh, S. H. Im, J. H. Heo, T. N. Mandal, S. I. Seok, *Nano Lett.* **2013**, *13*, 1764.

[7] Y. Jiao, S. Zhang, Z. Yang, G. Lu, *Comput. Theor. Chem.* **2019**, *1148*, 55.
[8] D. P. McMeekin, G. Sadoughi, W. Rehman, G. E. Eperon, M. Saliba, M. T. Hörantner, A. Haghighirad, N. Sakai, L. Korte, B. Rech, M. B. Johnston, L. M. Herz, H. J. Snaith, *Science* **2016**, *351*, 151.
[9] K. X. Steirer, P. Schulz, G. Teeter, V. Stevanovic, M. Yang, K. Zhu, J. J. Berry, *ACS Energy Lett.* **2016**, *1*, 360.
[10] H. Huang, M. I. Bodnarchuk, S. V. Kershaw, M. V. Kovalenko, A. L. Rogach, *ACS Energy Lett.* **2017**, *2*, 2071.
[11] P. Schulz, E. Edri, S. Kirmayer, G. Hodes, D. Cahen, A. Kahn, *Energy Environ. Sci.* **2014**, *7*, 1377.
[12] S. Béchu, M. Ralaiarisoa, A. Etcheberry, P. Schulz, *Adv. Energy Mater.* **2020**, *10*, 1904007.
[13] S. Wang, T. Sakurai, W. Wen, Y. Qi, *Adv. Mater. Interfaces* **2018**, *5*, 1800260.
[14] J. Endres, D. A. Egger, M. Kulbak, R. A. Kerner, L. Zhao, S. H. Silver, G. Hodes, B. P. Rand, D. Cahen, L. Kronik, A. Kahn, *J. Phys. Chem. Lett.* **2016**, *7*, 2722.
[15] E. M. Miller, Y. Zhao, C. C. Mercado, S. K. Saha, J. M. Luther, K. Zhu, V. Stevanović, C. L. Perkins, J. van de Lagemaat, *Phys. Chem. Chem. Phys.* **2014**, *16*, 22122.
[16] P. Schulz, L. L. Whittaker-Brooks, B. A. MacLeod, D. C. Olson, Y.-L. Loo, A. Kahn, *Adv. Mater. Interfaces* **2015**, *2*, 1400532.
[17] F. Zu, P. Amsalem, M. Ralaiarisoa, T. Schultz, R. Schlesinger, N. Koch, *ACS Appl. Mater. Interfaces* **2017**, *9*, 41546.
[18] M. Ralaiarisoa, I. Salzmann, F.-S. Zu, N. Koch, *Adv. Electron. Mater.* **2018**, *4*, 1800307.
[19] F.-S. Zu, P. Amsalem, I. Salzmann, R.-B. Wang, M. Ralaiarisoa, S. Kowarik, S. Duhm, N. Koch, *Adv. Opt. Mater.* **2017**, *5*, 1700139.
[20] J. D. McGettrick, K. Hooper, A. Pockett, J. Baker, J. Troughton, M. Carnie, T. Watson, *Mater. Lett.* **2019**, *251*, 98.
[21] W.-C. Lin, W.-C. Lo, J.-X. Li, Y.-K. Wang, J.-F. Tang, Z.-Y. Fong, *Npj Mater. Degrad.* **2021**, *5*, 1.
[22] L. Kronik, Y. Shapira, *Surf. Sci. Rep.* **1999**, *37*, 1.
[23] I. S. Zhidkov, D. W. Boukhvalov, A. F. Akbulatov, L. A. Frolova, L. D. Finkelstein, A. I. Kukharenko, S. O. Cholakh, C.-C. Chueh, P. A. Troshin, E. Z. Kurmaev, *Nano Energy* **2021**, *79*, 105421.
[24] V. Milotti, S. Cacovich, D. R. Ceratti, D. Ory, J. Barichello, F. Matteocci, A. Di Carlo, P. M. Sheverdyaeva, P. Schulz, P. Moras, *Small Methods* **2023**, 2300222.
[25] G. El-Hajje, C. Momblona, L. Gil-Escrig, J. Ávila, T. Guillemot, J.-F. Guillemoles, M. Sessolo, H. J. Bolink, L. Lombez, *Energy Environ. Sci.* **2016**, *9*, 2286.
[26] R. L. Z. Hoye, P. Schulz, L. T. Schelhas, A. M. Holder, K. H. Stone, J. D. Perkins, D. Vigil-Fowler, S. Siol, D. O. Scanlon, A. Zakutayev, A. Walsh, I. C. Smith, B. C. Melot, R. C. Kurchin, Y. Wang, J. Shi, F. C. Marques, J. J. Berry, W. Tumas, S. Lany, V. Stevanović, M. F. Toney, T. Buonassisi, *Chem. Mater.* **2017**, *29*, 1964.
[27] M. B. Trzhaskovskaya, V. I. Nefedov, V. G. Yarzhemsky, *At. Data Nucl. Data Tables* **2001**, *77*, 97.
[28] M. B. Trzhaskovskaya, V. I. Nefedov, V. G. Yarzhemsky, *At. Data Nucl. Data Tables* **2002**, *82*, 257.
[29] M. P. Seah, *Surf. Interface Anal.* **1980**, *2*, 222.
[30] S. Cacovich, D. Messou, A. Bercegol, S. Béchu, A. Yaiche, H. Shafique, J. Rousset, P. Schulz, M. Bouttemy, L. Lombez, *ACS Appl. Mater. Interfaces* **2020**, *12*, 34784.
[31] P. Schulz, D. Cahen, A. Kahn, *Chem. Rev.* **2019**, DOI 10.1021/acs.chemrev.8b00558.
[32] M. C. Brennan, S. Draguta, P. V. Kamat, M. Kuno, *ACS Energy Lett.* **2018**, *3*, 204.

[33] E. T. Hoke, D. J. Slotcavage, E. R. Dohner, A. R. Bowring, H. I. Karunadasa, M. D. McGehee, *Chem. Sci.* **2014**, *6*, 613.
[34] G. Sadoughi, D. E. Starr, E. Handick, S. D. Stranks, M. Gorgoi, R. G. Wilks, M. Bär, H. J. Snaith, *ACS Appl. Mater. Interfaces* **2015**, *7*, 13440.
[35] S. Olthof, K. Meerholz, *Sci. Rep.* **2017**, *7*, 40267.
[36] J. Ferrer Orri, T. A. S. Doherty, D. Johnstone, S. M. Collins, H. Simons, P. A. Midgley, C. Ducati, S. D. Stranks, *Adv. Mater.* **2022**, *34*, 2200383.